Measuring Galaxy Velocity Dispersions with Hectospec

Daniel	Fabricant,	Igor	Chilingarian,	Ho Seong	Hwang,	Michael	J.	Kurtz	and	Margaret	J.

Geller

Center for Astrophysics, Cambridge, MA 02138

Ian P. Del'Antonio

Brown University, Providence, RI 02912

Kenneth J. Rines

Western Washington University, Bellingham, WA 98225

Received	accepted

ABSTRACT

We describe a robust technique based on the ULySS IDL code for measuring velocity dispersions of galaxies observed with the MMT's fiber-fed spectrograph, Hectospec. This procedure is applicable to all Hectospec spectra having a signal-to-noise $\gtrsim 5$ and weak emission lines. We estimate the internal error in the Hectospec velocity dispersion measurements by comparing duplicate measurements of 171 galaxies. For a sample of 984 galaxies with a median z=0.10, we compare velocity dispersions measured by Hectospec through a 1.5'' diameter optical fiber with those measured by the Sloan Digital Sky Survey (SDSS) and Baryon Oscillation Spectral Survey (BOSS) through 3" and 2" diameter optical fibers, respectively. The systematic differences between the Hectospec and the SDSS/BOSS measurements are <7% for velocity dispersions between 100 and 300 km s⁻¹, the differences are no larger than the differences among the three BOSS velocity dispersion reductions. We analyze the scatter about the fundamental plane and find no significant redshift dependent systematics in our velocity dispersion measurements to $z\sim0.6$. This analysis also confirms our estimation of the measurement errors. In one hour in good conditions, we demonstrate that we achieve 30 km s⁻¹ velocity dispersion errors for galaxies with an SDSS r fiber magnitude of 21.

Subject headings: techniques: spectroscopic, galaxies: absorption lines, galaxies: emission lines

1. INTRODUCTION

Measurements of stellar velocity dispersions in galaxies have broad application including estimation of galaxy masses, galaxy classification, and distance measurements. The use of velocity dispersion measurements to determine galaxy properties and their evolution requires a clear understanding of the statistical and systematic errors in these measurements over a wide redshift range. Comparison of large samples of measurements obtained with different instruments and different techniques constrains these errors.

These broad applications of stellar velocity dispersion in galaxies motivate our investigation of velocity dispersion measurements from moderate to low signal-to-noise (SN) spectra originally obtained for redshift measurements. Hectospec, the MMT's fiber-fed spectrograph (Fabricant et al. 2005), has obtained spectra of ~700,000 unique objects; an appreciable fraction of these spectra can yield reliable velocity dispersions. Hectospec's fibers subtend 1.5" on the sky. Most spectra, obtained with a 270 line mm⁻¹ grating, have 5 Å FWHM resolution. We discuss results obtained with direct spectral fitting, an approach first described by Rix & White (1992). Direct spectral fitting is conceptually straightforward and allows simple masking of portions of the spectrum contaminated with strong skylines, bad pixels, or emission lines. We use a IDL-based software package, ULySS, developed by Koleva et al. (2009) to perform direct fitting of Hectospec spectra. ULySS fits observed spectra to model spectra of synthesized galaxy stellar populations broadened by the instrumental line spread function and a velocity dispersion.

An extensive literature reporting velocity dispersion techniques and measurements follows the pioneering work of Minkowski (1954) who reported measurements of M31's velocity dispersion. The earliest measurements using optical fiber front-ends were performed at the AAT (Colless & Hewett 1987; Lucey & Carter 1988). Jørgensen, Franx, & Kjærgaard (1995) made extensive comparisons of velocity dispersions from the fiber-fed OCTOPUS

spectrograph with slit spectrograph measurements, and obtained consistent results. Beginning with the first data release (Abazajian et al. 2003), the Sloan Digital Sky Survey (SDSS) has made available extensive catalogs of well-calibrated velocity dispersions obtained with fiber-fed spectrographs. The only serious disadvantage of measuring velocity dispersions through fibers rather than directly with a slit spectrograph is the sacrifice of spatial resolution for multiplex advantage.

In Section 2 we describe application of ULySS to Hectospec spectra with weak nebular line emission allowing uncontaminated measurement of stellar absorption features. We calculate the internal errors in our velocity dispersion measurements in Section 3. In Section 4 we compare our velocity dispersion measurements for 984 galaxies with SDSS/Baryon Oscillation Spectral Survey (BoSS) Date Release 9 (DR9) pipeline measurements. We plot the scatter about the fundamental plane for a sample of 1857 galaxies to a redshift of 0.6 in Section 5 to demonstrate that our velocity dispersion errors are accurate at higher redshifts. We describe how to plan velocity dispersion measurements with Hectospec in Section 6, and give our conclusions in Section 7. We adopt cosmological parameters $H_0=70$, $\Omega_M=0.3$, and $\Omega_{\Lambda}=0.7$.

2. Hectospec Velocity Dispersion Measurements

2.1. Introduction

The ULySS algorithms (Koleva et al. 2009) are based on an earlier IDL package, NBURSTS, developed by Chilingarian et al. (2007). NBURSTS in turn is based on the pPXF package developed by Cappellari & Emsellem (2004). ULySS simultaneously fits a spectrum with the internal galaxy dynamics and parameters describing a star formation history. To extract accurate velocity dispersions, the model spectrum must be convolved

to the same wavelength dependent spectral resolution as the data. ULySS then applies a multiplicative polynomial to account for errors in flux calibration of the data and for inaccuracies in the model prediction.

The galaxy spectral models we use are single age stellar populations (SSP) parameterized by age and metallicity. We used a precomputed grid of SSP models (Prugniel, Vauglin & Koleva 2011) calculated with the PegaseHR code (Le Borgne et al. 2004) from the MILES stellar library (Sanchez-Blazquez et al. 2006), assuming a Salpeter initial mass function and solar neighborhood abundances. This grid of models is available on the ULyss web site (ulyss.univ-lyon1.fr). We adopt a cosmology with $H_0=70$, $\Omega_M=0.3$, and $\Omega_{\Lambda}=0.7$.

2.2. ULySS Parameters

The first step in our analysis is relative flux calibration of the Hectospec spectra following the techniques described in Fabricant et al. (2008). We write out the deredshifted fluxed spectra in a FITS format compatible with ULySS. As described in Fabricant et al. (2008), the flux calibration is quite stable over time, and the ULySS multiplicative polynomial accounts for any small errors in flux calibration.

We experimented extensively with the available ULySS parameters. We obtain the lowest velocity dispersion errors and stablest results by restricting the spectral range to 4100-5500 Å, by restricting the model metallicities $(\log(\frac{model}{solar}))$ between -0.5 and 0.5, and by using a third order multiplicative polynomial. Accessing lower metallicities in model fits allows an unphysical degeneracy between age and metallicity for low SN spectra (Worthey 1995). Higher order multiplicative polynomials do not meaningfully reduce chi squared and sometimes attempt to null real spectral features on low SN spectra.

2.3. Hectospec's Line Spread Function

We determine Hectospec's line spread function (LSF) using the ULySS routine uly_lsf. This routine derives the line spread function by fitting twilight flat spectra to a high resolution model (R=10000) of the solar spectrum provided in the ULySS distribution. As supplied, uly_lsf fits only a velocity shift and a Gaussian LSF, but is easily modified to fit h3 and h4 Hermite polynomials to describe a non-Gaussian LSF. Although Hectospec's optical fibers do provide a somewhat flat topped LSF, measurements of h3 and h4 with uly_lsf scatter closely about 0. We therefore fix the h3 and h4 terms at zero.

Hectospec's fiber feed guarantees a consistent input aperture, and the line spread function should be quite stable; the only time dependent changes should arise from focus variations and changes in the fiber focal ratio degradation. The Hectospec focus is regularly checked and is maintained within a tight range, and Hectospec was carefully designed to minimize focal ratio degradation (Fabricant et al. 2005). In addition to time dependent changes, variation in the image quality of Hectospec's optics and the flatness and alignment of the CCD detectors can introduce fiber to fiber variations in the line spread function. These spatially and time dependent variations in the line spread function can be recovered from the twilight flats for each night of data and each fiber. A new pipeline under development will correct for these issues. We show that very acceptable results can be obtained from the current pipeline by using a line spread function averaged over fiber and time.

We have measured the Hectospec line spread function for each of the 300 fibers on three randomly chosen nights: 13 October 2007, 20 November 2008, and 15 October 2009. For these 900 measurements we calculate the LSF in 17 wavelength bins, each 200 Å wide, centered between 3800 to 8900 Å. For each bin, we calculate the mean Gaussian (1 σ) LSF in km s⁻¹ and the standard deviation in the LSF. The LSF ranges between 172 km s⁻¹

at 3800 Å, 105 km s⁻¹ at 6000 Å, and 78 km s⁻¹ at 9000 Å, or 5.1, 4.9, 5.5 Å FWHM, respectively. The standard deviation in these measurements is typically 3 km s⁻¹, or 2% of the LSF at the blue end and 5% of the LSF at the red end of Hectospec's spectral range. These standard deviations are small enough to support use of the average LSF. Spectral regions affected by strong atmospheric absorption (particularly between 6800 and 7600 Å) yield incorrect LSFs from the twilight flats and must be rejected. We fit a third order polynomial to the valid data points; the coefficients of the fit are in Table 1.

To analyze the fluxed Hectospec spectra shifted to rest frame wavelengths, we use the LSF appropriate to the original observed wavelengths. In addition, we correct for the intrinsic resolution of the MILES stellar library, 2.51 Å FWHM (Falcón-Barroso et al. 2011), or σ =1.066 Å (see also Prugniel, Vauglin & Koleva (2011); Beifiori et al. (2011)). We subtract this resolution in quadrature from the redshift-shifted Hectospec LSF to produce a final LSF for each spectrum. Figure 1 shows sample Hectospec spectra with the ULySS fits overplotted.

3. Internal Errors

We examine the internal errors in our velocity dispersions using a sample of 171 pairs of measurements from the SHELS survey (Geller et al. 2010) where the error in each measurement is $<30 \text{ km s}^{-1}$. Figure 2 is a histogram of the dispersion differences in km s⁻¹. The expected RMS dispersion difference calculated from the ULySS errors is 21.7 km s⁻¹, we measure an RMS dispersion difference of 20.5 km s⁻¹ for the 171 pairs. We show Gaussian of 18 km s⁻¹ σ fit to the binned data for reference in Figure 2. Our repeated measurements confirm the ULySS error estimates, and we adopt these errors for subsequent analysis.

4. External Errors - Comparison with SDSS/BOSS DR9

We assess our external errors using Hectospec velocity dispersion measurements for a sample of 984 galaxies with high SN velocity dispersion measurements (estimated dispersion errors $<20 \text{ km s}^{-1}$ in both cases) in the 9th SDSS/Baryon Oscillation Spectroscopic Survey (BOSS) data release (DR9, Ahn et al. (2012)); 843 of these spectra were obtained with the SDSS fiber-fed spectrographs and 141 with the updated BOSS fiber-fed spectrographs (Smee et al. 2013). The median redshift of the combined sample is 0.147. Galaxies with [OII] λ 3727 equivalent widths >5Å were excluded from this sample to avoid contamination from emission lines.

The Hectospec spectra are drawn from three surveys: SHELS (Geller et al. 2010, 2012; Hwang & Geller 2013), the Hectospec Cluster Survey(HeCS) (Rines et al. 2013), and HectoMap (Geller et al. 2011). These surveys include $\sim 15,000$, $\sim 22,000$, and $\sim 52,000$ Hectospec spectra, respectively, all with the same Hectospec configuration. SHELS is a magnitude limited survey complete to R=20.6; here we use the entire sample including some galaxies fainter than the R=20.6 limit. HeCS surveys red sequence galaxies with r<21 in 58 galaxy clusters. HectoMAP is a survey of red selected galaxies in a 50 deg² strip to r<21.3. By design, only a small fraction of these galaxies overlap with one of the SDSS surveys.

The SDSS-I/II fibers subtend 3", the SDSS-III/BOSS fibers subtend 2". To compare the Hectospec measurements directly with the DR9 velocity dispersions, we apply an aperture correction to scale the Hectospec velocity dispersions downwards to match the larger SDSS or BOSS apertures. We use the aperture correction from Cappellari et al. (2006):

$$\frac{\sigma_1}{\sigma_2} = \left(\frac{r_1}{r_2}\right)^{-0.066}$$

The aperture corrections to transform to the SDSS and BOSS apertures are thus 0.955 and 0.981, respectively. Figure 3 shows the 984 pairs of Hectospec and DR9 (Bolton et al. 2012) pipeline velocity dispersions. We remove two galaxies from analysis with dispersions that disagree by more than 5 σ . Although the two measurements of independent spectra analyzed with rather different software show remarkable agreement, it is clear that the Hectospec/ULySS velocity dispersions are systematically larger at large dispersions. The solid line in Figure 3 shows the error-weighted best fit line relating the two measurements; the line (valid only between 100 and 300 km s⁻¹) has an intercept of -20.5 km s⁻¹ and a slope of 1.139.

We can also study the error distribution. The expected RMS dispersion difference calculated from the ULySS and DR9 pipeline errors is 17.1 km s⁻¹, but we measure a larger RMS dispersion difference of 24.7 km s⁻¹ for the 984 pairs. Here, we have removed the linear relation described above. The measured RMS dispersion difference suggests that the errors are underestimated by $\sqrt{2}$. However, various systematic errors like aperture centration and aperture corrections probably contribute. Because our repeated measurements agree within the ULySS errors, systematic errors may dominate the apparent excess error.

We next consider the systematic differences in velocity dispersions. We can explore the effect of different velocity dispersion analysis techniques by comparing the three BOSS DR9 reductions; the pipeline reduction (Bolton et al. 2012), the Portsmouth reduction (Thomas et al. 2013), and the Wisconsin reduction (Chen et al. 2012). Figure 4 shows the velocity dispersions of the subset of 12759 BOSS galaxies with velocity dispersion errors of $<10 \text{ km s}^{-1}$ in both analyses. The solid line in Figure 3 shows the error-weighted best fit line relating the two measurements; the line (valid only between 100 and 300 km s⁻¹) has an intercept of -10.4 km s⁻¹ and a slope of 1.093. The systematic difference between the two analyses is negligible at 100 km s⁻¹, rising to $\sim6\%$ at 300 km s⁻¹. Figure 5 shows the

velocity dispersions of the subset of 6638 BOSS galaxies with velocity dispersion errors of $<20~\rm km~s^{-1}$ in both analyses. The solid line in Figure 3 shows the error-weighted best fit line relating the two measurements; the line (valid only between 100 and 300 km s⁻¹) has an intercept of 15.6 km s⁻¹ and a slope of 0.947. The systematic difference between the two analyses is $\sim10\%$ at 100 km s⁻¹, and negligible at 300 km s⁻¹. Thomas et al. (2013) presents plots comparing the various DR9 BOSS reductions with a less restrictive cut on the velocity dispersion errors.

Table 2 summarizes the ratios of the velocity dispersions from the Hectospec analysis, the Portsmouth, and the Wisconsin reductions relative to the DR9 pipeline. The DR9 reductions reflect only differing analysis techniques; the underlying spectra are identical. It is interesting to note that the systematic deviations of the Hectospec/ULySS velocity dispersions relative to the DR9 pipeline are almost identical to those of the Portsmouth reductions relative to the DR9 pipeline. The Portsmouth analysis uses the pPXF (Cappellari & Emsellem 2004) code that is functionally identical to ULySS and very similar stellar population models. In contrast, both the Wisconsin and pipeline analyses use some form of principal component analysis. We conclude that the systematic differences between Hectospec and DR9 pipeline dispersions are no larger than the differences among the three different DR9 reductions.

5. External Validation Using the Fundamental Plane

Night sky features contribute differently to velocity dispersion errors as a function of the redshift of the measured galaxy. The MgI b triplet at low redshift is in a spectral region where the night sky is relatively smooth and easily subtracted; at a redshift of 0.6 this feature is well inside the "forest" of OH night-sky emission lines. The direct external validation by comparison with the SDSS in section 4 does not contain a sufficient number of

high redshift objects to show the presence or absence of systematic tendencies at redshifts above $z \sim 0.2$. We perform an indirect validation by observing the scatter and offset about the fundamental plane as a function of redshift.

It has long been known (Faber & Jackson 1976; Djorgovski & Davis 1987) that early type galaxies define a narrow relation in velocity dispersion (σ), surface brightness (μ) and effective radius (r_e), the fundamental plane (FP).

$$log(r_e) = alog(\sigma) + b\mu + c$$

We use this relation to test for redshift dependant systematics in the dispersions and their errors. Previous studies have shown: (1) that the FP parameterization does not vary with redshift, at least for z≤0.6 (Kelson et al. 1997; Jørgensen, Franx, & Kjærgaard 1996; van Dokkum & Franx 1996) and (2) that the intrinsic scatter about the FP relation is stable (Hyde & Bernardi 2009).

We use spectral measurements from the SHELS survey (Geller et al. 2010) and photometric measurements from the SDSS DR9 (Ahn et al. 2012) to make that test. We adopt the r band C-model FP calibration of Saulder et al. (2013) (a=1.041, b= 0.30 c=-7.76) which uses cModelMag_r and deVRad_r, and we follow their prescription almost exactly for correcting the input measures for aperture differences, the k correction, and evolution. The two differences from their analysis are: (1) that we do not correct the measured radius of each galaxy for its ellipticity, and (2) for redshifts from 0.5 to 0.6 we use an extrapolation of the modified k correction of Chilingarian et al. (2010) used by Saulder et al. (2013). Our extrapolation assumes an elliptical galaxy spectrum.

We choose "red" galaxies by requiring that deVfrac_r >0.6 and OII 3727 emission <5 Å and $D_{\lambda}4000 >1.65$. In addition we require a fractional error in the velocity dispersion <20%. Figure 6 shows the residuals in the FP as a function of redshift. We show all 1857 objects which pass the selection. The mean offset is 0.0011 with a standard deviation of

0.1181. We compute the number of objects, the mean offset and the standard deviation in three redshift bins: (0 < z < 0.25; n=719; offset=0.0077; s.d.=0.1176), (0.25 < z < 0.25); n=600; offset=-0.0020, s.d.=0.1195), (0.35 < z < 0.60; n=483; offset=-0.0075, s.d.=0.1211). The offsets of the whole sample and the redshift selected subsamples are consistent with zero. Thus there is no significant redshift dependent error in the measured velocity dispersions.

We externally validate the errors in the velocity dispersion measurements by computing the intrinsic scatter in the FP with two different cuts in fractional velocity dispersion error. Because we compute the intrinsic width of the FP by subtracting (in quadrature) the error expected by propagating the individual measurement errors from the measured scatter, under(over) estimates of the measurement errors will produce a computed intrinsic width that differs for samples with different error cuts.

To eliminate any redshift dependent effects we narrow our analysis to the central redshift bin: 0.25<z<0.35. We compute the FP intrinsic width from two samples: (1) galaxies with a maximum fractional dispersion error of 0.20, and (2) galaxies with a fractional dispersion error <0.10. For the 20% error sample we compute an intrinsic width of 0.0999 from 600 galaxies; for the 10% error sample we compute an intrinsic width of 0.1008 from 182 galaxies. The difference in the computed widths is small. If the difference resulted entirely from a misestimation of the velocity dispersion errors, the errors would have to be overestimated by 5%, in basic agreement with the internal error analysis in section 3.

6. Planning Hectospec Dispersion Measurements

Here we compute the velocity dispersion errors expected as a function of magnitude for an exposure time of 3600 s. We have insufficient experience with significantly longer exposures to determine the errors as a function of exposure time.

We examine a sample of 1262 SHELS galaxies observed for 3600 s with velocity dispersion errors <50 km s⁻¹. We expect the errors to correlate best with 1.5" aperture magnitudes corresponding to the Hectospec fiber diameter. Figure 7 plots the Hectospec velocity dispersion errors as a function of R magnitude in a 1.5" aperture (Wittman et al. 2002, 2006). The correlation reflects a range of observing conditions including seeing, cloud cover, and moon illumination. The lower envelope of the distribution corresponds to observations during dark conditions with good seeing and clear skies. Under these conditions, with a 3600 s observation we expect a 20 km s⁻¹ velocity dispersion error for a galaxy with an R aperture magnitude of 20.5, and a 30 km s⁻¹ velocity dispersion error for a galaxy with an R aperture magnitude of 21.

For most observers, the best easily available proxy for Hectospec fiber magnitudes is SDSS fiber magnitudes measured in a 3" aperture. These magnitudes do not correlate as well with the Hectospec velocity dispersion errors as the 1.5" aperture magnitudes (Figure 7), but they are still useful (Figure 8). Under the best conditions, we expect a 20 km s⁻¹ velocity dispersion error for a galaxy with an r SDSS fiber magnitude of 20.4, and a 30 km s⁻¹ velocity dispersion error for a galaxy with an r fiber magnitude of 21. The differences in filter bandpass and aperture roughly cancel.

7. Conclusions

The main goal of our investigation is to enable studies of fundamental galaxy properties and their evolution using Hectospec data. Careful comparisons of velocity dispersion measurements made with independent instruments are also of more general interest to establish the accuracy of our large data sets in an era of "precision cosmology".

-14-

We describe the use of publicly available software, ULySS (Koleva et al. 2009), to

obtain velocity dispersions for Hectospec galaxy spectra. We compare our measurements

to those from the SDSS DR9 pipeline for 984 galaxies in common with velocity dispersion

errors of $<20 \text{ km s}^{-1}$. The systematic differences in the two measurements are <7% for

galaxies with dispersions between 100 and 300 km s⁻¹. These differences are comparable

to the systematic differences among the three velocity dispersion reductions for the DR9

BOSS data.

By analyzing the scatter about the fundamental plane we show that there are no

significant systematics in our velocity dispersion measures as a function of redshift, for

z≤0.6. Additionally we confirm that our estimation of the measurement errors is correct,

within narrow tolerances.

In one hour in good conditions, we can expect 20 km s⁻¹ velocity dispersion errors for

a galaxy with an r SDSS fiber magnitude of 20.4, and 30 km s⁻¹ velocity dispersion errors

for a galaxy with an r fiber magnitude of 21.

Facility: MMT (Hectospec)

ACKNOWLEDGMENTS 8.

We thank Marijn Franx, Nelson Caldwell and Daniel Eisenstein for helpful comments.

Observations reported here were obtained at the MMT Observatory, a joint facility

of the Smithsonian Institution and the University of Arizona. We thank the Hectospec

engineering team including Robert Fata, Tom Gauron, Marc Lacasse, Mark Mueller,

and Joe Zajac, and the instrument specialists Perry Berlind and Michael Calkins. We

are grateful for the contributions of the members of the CfA's Telescope Data Center

including Warren Brown, Anne Matthews, John Roll, Susan Tokarz and Sean Moran.

The entire staff of the MMT Observatory under the direction of G. Grant Williams has provided outstanding support for Hectospec operations. Nelson Caldwell has ably scheduled Hectospec's queue operations.

Funding for the SDSS and SDSS-II has been provided by the Alfred P. Sloan Foundation, the Participating Institutions, the National Science Foundation, the U.S. Department of Energy, the National Aeronautics and Space Administration, the Japanese Monbukagakusho, the Max Planck Society, and the Higher Education Funding Council for England. The SDSS Web Site is http://www.sdss.org/. The SDSS is managed by the Astrophysical Research Consortium for the Participating Institutions. Funding for SDSS-III has been provided by the Alfred P. Sloan Foundation, the Participating Institutions, the National Science Foundation, and the U.S. Department of Energy Office of Science. The SDSS-III web site is http://www.sdss3.org/.

REFERENCES

Abazajian, K. et al. 2003, AJ, 126, 2081

Ahn, C. P., 2012, ApJS, 203, 21

Beifiori, A. et al. 2011, A&A, 531, 109

Bolton, A. et al. 2012, AJ, 144, 144

Chen, Y.-M. et al. 2012, MNRAS, 421, 314

Cappellari, M. & Emsellem, E. 2004, PASP, 116, 138

Cappellari, M. et al. 2006, MNRAS, 366, 1126

Chilingarian, I. et al. 2007, in IAU Symp. 241, 175

Chilingarian, I. et al. 2010, MNRAS, 405, 1409

Colless, M. & Hewett, P. 1987, MNRAS, 224, 453

Djorgovski, S., & Davis, M. 1987, ApJ, 313, 59

Fabricant, D., et al. 2005, PASP, 117, 1411

Faber, S. M., & Jackson, R. E. 1976, ApJ, 204, 668

Fabricant et al. 2008, PASP, 120, 1222

Falcón-Barroso, J. et al. 2011, A&A, 532, 95

Geller, M. J. et al. 2010, ApJ, 709, 832

Geller, M. J., Diaferio, A., & Kurtz, M. J. 2011, AJ, 142, 133

Geller, M. J. et al. 2012, AJ, 143, 102

Hyde, J. B., & Bernardi, M. 2009, MNRAS, 396, 1171

Hwang, H. S. & Geller, M. J. 2013, ApJ, 769, 116

Jørgensen, I., Franx, M., & Kjærgaard, P. 1995, MNRAS, 276, 1341

Jørgensen, I., Franx, M., & Kjærgaard, P. 1996, MNRAS, 280, 167

Kelson, D. D. et al. 1997, ApJ, 478, L13

Le Borgne, D. et al. 2004, A&A, 425, 881

Koleva, M. et al. 2009, A&A, 501, 1269

Lucey, J.R. & Carter, D. 1988, MNRAS, 235, 1177

Minkowski, 1954, Carnegie Yearbook, 26

Prugniel, P., Vauglin, I., & Koleva, M. 2011, A&A, 521, 165

Rines, K. et al. 2013, ApJ, 767, 15

Rix, H.-W. & White, S. 1992, MNRAS, 254, 389

Sanchez-Blazquez, P. 2006, MNRAS, 371, 703

Saulder, C., et al. 2013, arXiv:1306.0285

Smee, S. et al. 2013, AJ, in press

Thomas, D. et al. 2013, MNRAS, 431, 1383

van Dokkum, P. G., & Franx, M. 1996, MNRAS, 281, 985

Wittman, D. M., et al. 2002, Proc. SPIE, 4836, 73

Wittman, D., et al. 2006, ApJ, 643, 128

Worthey, G. 1995, ApJS, 95, 107

This manuscript was prepared with the AAS $\mbox{\sc int} T_{\mbox{\sc E\!\!\!/}} X$ macros v5.2.

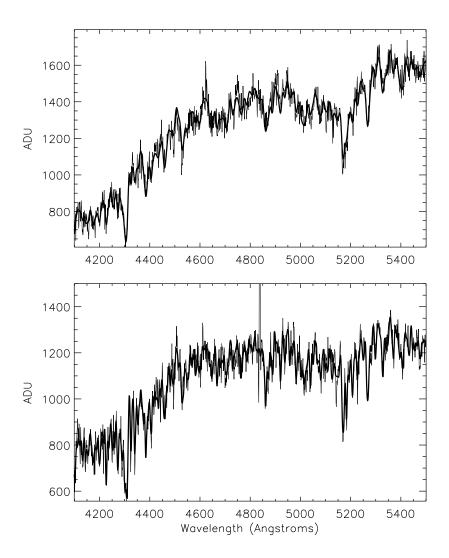


Fig. 1.— Sample ULySS fits (bold line) overplotted on Hectospec spectra (fine line). The spectrum in the bottom panel yields a velocity dispersion of 101 ± 6 km s⁻¹ and the spectrum in the top panel yields a velocity dispersion of 281 ± 8 km s⁻¹.

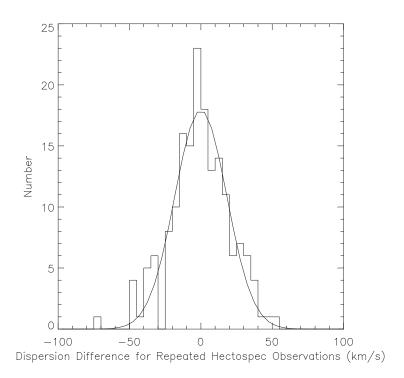


Fig. 2.— Hectospec internal velocity dispersion differences for repeated measurements of 171 galaxies where the error in each measurement is $<30~\rm km~s^{-1}$. The expected RMS dispersion difference calculated from the errors is 22 km s⁻¹ and the measured RMS difference is 21 km s⁻¹. A Gaussian of 18 km s⁻¹ σ fit to the binned data is shown for reference.

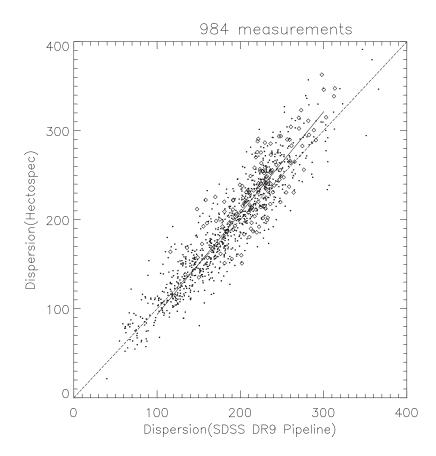


Fig. 3.— A comparison of independent Hectospec and SDSS measurements of 984 galaxies with velocity dispersion errors <20 km s⁻¹. An aperture correction has been applied to the Hectospec data (see text). The short solid line segment is a error weighted fit of a line to the plotted data points. This line has an intercept of -20.5 and a slope of 1.139. Measurements with the original SDSS spectrograph and 3" fibers are plotted with filled symbols (843 galaxies) and measurements with the updated BOSS spectrograph with 2" fibers are plotted with open symbols (141 galaxies).

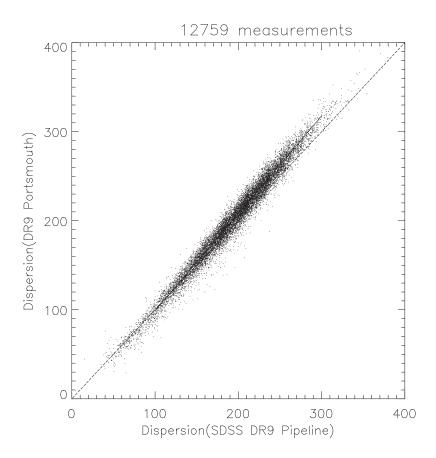


Fig. 4.— A comparison of DR9 Portsmouth and DR9 pipeline measurements of 12759 galaxies with velocity dispersion errors $<10 \text{ km s}^{-1}$. The short solid line segment is a error weighted fit of a line to the plotted data points. This line has an intercept of -10.4 and a slope of 1.093.

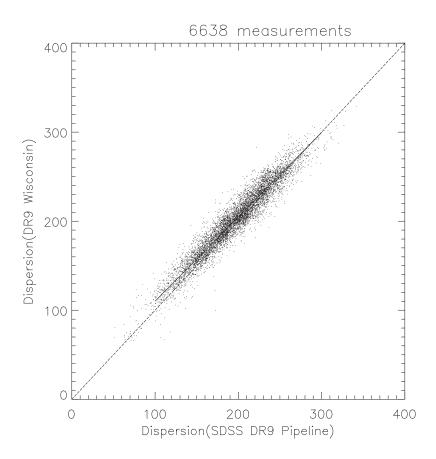


Fig. 5.— A comparison of DR9 Wisconsin and DR9 pipeline measurements of 6638 galaxies with velocity dispersion errors $<20 \text{ km s}^{-1}$. The short solid line segment is a error weighted fit of a line to the plotted data points. This line has an intercept of 15.6 and a slope of 0.947.

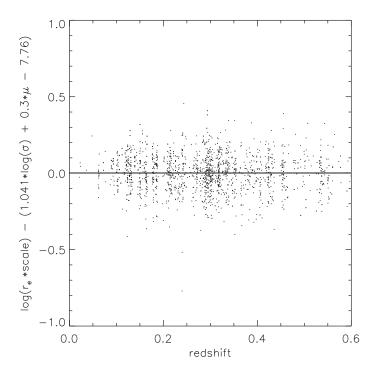


Fig. 6.— The scatter of 1857 galaxies from the SHELS survey (Geller et al. 2010) about the C-model fundamental plane relationship of Saulder et al. (2013) as a function of redshift. Here r_e is deVRad_r and μ is computed as $\mu = 2.5log(2\pi) + 5log(r_e) + cModelMag_r$. The sample selection is described in the text.

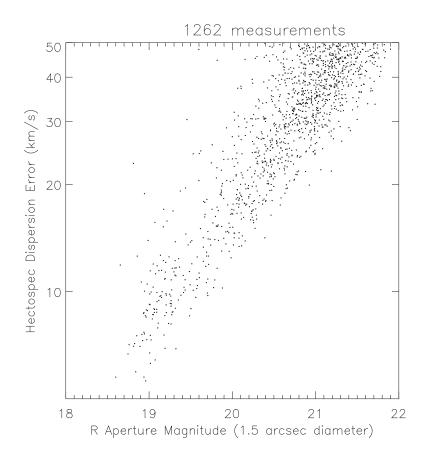


Fig. 7.— Hectospec velocity dispersion errors for a 3600 s observation as a function of R magnitude within a 1.5" Hectospec fiber aperture. The points reflect observations of galaxies with velocity dispersions between 100 and 300 km s⁻¹ during a wide range of conditions including seeing and transparency. Although we expect the errors to depend on the galaxy dispersion, this dependence is obscured by the seeing and transparency variations that we cannot accurately remove. The lower envelope reflects observations during the best conditions.

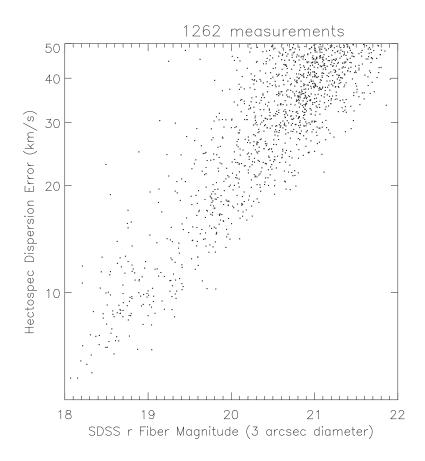


Fig. 8.— Hectospec velocity dispersion errors for a 3600 s observation as a function of r magnitude within a 3" aperture (SDSS fibermag). The points reflect observations during a wide range of conditions including seeing and transparency. The lower envelope reflects observations during the best conditions.

Table 1. Hectospec Line Spread Function (km $\rm s^{-1})$

Polynomial Term	Coefficient			
constant	4.64400×10^2			
linear	-1.15515×10^{-1}			
quadratic	1.16604×10^{-5}			
cubic	-3.99359×10^{-10}			

Table 2. Dispersion Ratios

DR9 Pipeline Dispersion(km s^{-1})	Hectospec Ratio	Portsmouth Ratio	Wisconsin Ratio
100	0.93	0.99	1.10
150	1.00	1.02	1.05
200	1.04	1.04	1.02
250	1.06	1.05	1.01
300	1.07	1.06	1.00